



# Reactive Gas Phase Compression Due to Shock-Induced Cavity Collapse in Energetic Materials

by Linhbao Tran

ARL-RP-179

June 2007

A reprint from the *Proceedings of the 13th International Symposium on Detonation*,  
Norfolk, VA, 23 July 2006.

## **NOTICES**

### **Disclaimers**

The findings in this report are not to be construed as an official Department of the Army position unless so designated by other authorized documents.

Citation of manufacturer's or trade names does not constitute an official endorsement or approval of the use thereof.

Destroy this report when it is no longer needed. Do not return it to the originator.

# **Army Research Laboratory**

Aberdeen Proving Ground, MD 21005-5069

---

---

**ARL-RP-179**

**June 2007**

---

---

## **Reactive Gas Phase Compression Due to Shock-Induced Cavity Collapse in Energetic Materials**

**Linhbao Tran**

**Weapons and Materials Research Directorate, ARL**

*A reprint from the Proceedings of the 13th International Symposium on Detonation,  
Norfolk, VA, 23 July 2006.*

REPORT DOCUMENTATION PAGE			Form Approved OMB No. 0704-0188		
Public reporting burden for this collection of information is estimated to average 1 hour per response, including the time for reviewing instructions, searching existing data sources, gathering and maintaining the data needed, and completing and reviewing the collection information. Send comments regarding this burden estimate or any other aspect of this collection of information, including suggestions for reducing the burden, to Department of Defense, Washington Headquarters Services, Directorate for Information Operations and Reports (0704-0188), 1215 Jefferson Davis Highway, Suite 1204, Arlington, VA 22202-4302. Respondents should be aware that notwithstanding any other provision of law, no person shall be subject to any penalty for failing to comply with a collection of information if it does not display a currently valid OMB control number. <b>PLEASE DO NOT RETURN YOUR FORM TO THE ABOVE ADDRESS.</b>					
1. REPORT DATE (DD-MM-YYYY) June 2007		2. REPORT TYPE Reprint		3. DATES COVERED (From - To) September 2005–June 2006	
4. TITLE AND SUBTITLE Reactive Gas Phase Compression Due to Shock-Induced Cavity Collapse in Energetic Materials			5a. CONTRACT NUMBER		
			5b. GRANT NUMBER		
			5c. PROGRAM ELEMENT NUMBER		
6. AUTHOR(S) Linhbao Tran			5d. PROJECT NUMBER AH80		
			5e. TASK NUMBER		
			5f. WORK UNIT NUMBER		
7. PERFORMING ORGANIZATION NAME(S) AND ADDRESS(ES) U.S. Army Research Laboratory ATTN: AMSRD-ARL-WM-TB Aberdeen Proving Ground, MD 21005-5069			8. PERFORMING ORGANIZATION REPORT NUMBER ARL-RP-179		
9. SPONSORING/MONITORING AGENCY NAME(S) AND ADDRESS(ES)			10. SPONSOR/MONITOR'S ACRONYM(S)		
			11. SPONSOR/MONITOR'S REPORT NUMBER(S)		
12. DISTRIBUTION/AVAILABILITY STATEMENT Approved for public release; distribution is unlimited.					
13. SUPPLEMENTARY NOTES A reprint from the <i>Proceedings of the 13th International Symposium on Detonation</i> , Norfolk, VA, 23 July 2006.					
14. ABSTRACT A mesoscale simulation is carried out to examine shock-initiation due to gas phase reaction at site of cylindrical pore within an HMX crystal. The focus here is to investigate viscoplastic heating with gas pore compression that leads to chemical reactions within the gas phase. Systems of conservation laws for both solid and gas phases are solved along with species conservation from a reduced set of chemical kinetic model. Mass, momentum, and energy transfer between phases are applied explicitly at the solid-gas interface using physical boundary conditions, thus avoiding empiricism of mixture multiphase formulation. These transfer processes are critical in the Mach stem formation around the collapsing reacting gas pore.					
15. SUBJECT TERMS hot spot, void collapse, initiation, gas phase compression, reactive					
16. SECURITY CLASSIFICATION OF:			17. LIMITATION OF ABSTRACT  UL	18. NUMBER OF PAGES  16	19a. NAME OF RESPONSIBLE PERSON Linhbao Tran
a. REPORT UNCLASSIFIED	b. ABSTRACT UNCLASSIFIED	c. THIS PAGE UNCLASSIFIED			19b. TELEPHONE NUMBER (Include area code) 410-278-9757

# REACTIVE GAS PHASE COMPRESSION DUE TO SHOCK-INDUCED CAVITY COLLAPSE IN ENERGETIC MATERIALS

Linhbao Tran

U.S. Army Research Laboratory  
Aberdeen Proving Ground, MD 21005, U.S.A

**Abstract.** A mesoscale simulation is carried out to examine shock-initiation due to gas phase reaction at site of cylindrical pore within an HMX crystal. The focus here is to investigate viscoplastic heating with gas pore compression that leads to chemical reactions within the gas phase. Systems of conservation laws for both solid and gas phases are solved along with species conservation from a reduced set of chemical kinetic model. Mass, momentum, and energy transfer between phases are applied explicitly at the solid-gas interface using physical boundary conditions, thus avoiding empiricism of mixture multiphase formulation. These transfer processes are critical in the Mach stem formation around the collapsing reacting gas pore.

## INTRODUCTION

The initiation phenomenon in a heterogeneous energetic material, such as a plastic bonded explosive (PBX) is dominated [1] by the occurrence of hot spots at density discontinuities within the material. Initiation of an energetic material can occur when an impulse delivered to a high explosive material evolves into a detonation wave. Growth to detonation depends on the formation of localized regions of elevated thermal energy, or hot spots that have temperatures higher than the bulk temperature expected from shock heating. When sufficient thermal energy is generated locally, ignition occurs and subsequent chemical energy release, having overcome energy dissipation in the form of heat conduction, leads to progressive shock strengthening until detonation conditions are achieved. This concept was first proposed by Bowden and Yoffe [1].

A number of mechanisms for the formation of hot spots have been proposed over the years, such as frictional heating between adjacent grains [2-3],

hydrodynamic jetting [4], viscoplastic void collapse [5-7], and adiabatic gas pore compression [1,8-10]. The applicability of these mechanisms depends on the strength of the imposed shock, size of microstructure defects, material properties, etc. that initiates the explosion. Regimes of applicability can be identified roughly by the criterion proposed by Khasainov et al. [6].

In the current study, we investigate the effect of viscoplastic heating and gas pore compression of an idealized cylindrical pore due to the passage of a shock. The formulation involves solving both solid and gas phases separately using a sharp interface technique and shock capturing methodology. The coupling of the two phases is carried out by applying explicitly the physical boundary condition at the interface. A reduced chemical kinetic model [11-12] is implemented that includes three reactions with four lumped chemical species.

## FORMULATION

### Governing Equations

The two-dimensional mass, momentum, and energy conservation equations with additional transport equations for equivalent plastic strain and deviatoric stresses in the solid phase, are given generally as:

$$\bar{Q}_{,t} + F(\bar{Q})_{,x} + G(\bar{Q})_{,y} = S(\bar{Q}) \quad (1)$$

where vector of conserved variables is  $\bar{Q}$ , convective flux vectors are  $F(\bar{Q})$  and  $G(\bar{Q})$ , source term is  $S(\bar{Q})$ , and subscripts are derivatives with respect to temporal (t) and spatial directions (x and y).

The conservative variables and convective fluxes for gas phase are:

$$\bar{Q} = \{\rho, \rho u, \rho v, \rho E\} \quad (2)$$

$$F(\bar{Q}) = \{\rho u, \rho u^2 + p, \rho uv, u(\rho E + p)\} \quad (3)$$

$$G(\bar{Q}) = \{\rho v, \rho uv, \rho v^2 + p, v(\rho E + p)\} \quad (4)$$

For the solid phase, the deviatoric stresses are expressed in Jaumann rate [13] form:

$$\bar{Q} = \{\rho, \rho u, \rho v, \rho E, \rho \bar{\epsilon}_p, \rho s_{xx}, \rho s_{yy}, \rho s_{xy}\} \quad (5)$$

$$F(\bar{Q}) = \{\rho u, \rho u^2 + p, \rho uv, u(\rho E + p), \rho u \bar{\epsilon}_p, \rho u s_{xx}, \rho u s_{yy}, \rho u s_{xy}\} \quad (6)$$

$$G(\bar{Q}) = \{\rho v, \rho uv, \rho v^2 + p, v(\rho E + p), \rho v \bar{\epsilon}_p, \rho v s_{xx}, \rho v s_{yy}, \rho v s_{xy}\} \quad (7)$$

The dilatational component of the stress is obtained from the equation of state and is presented later. Symbols used here follow standard convention.

In addition to the usual viscous stresses and thermal conduction in the source terms, there are enthalpy fluxes due to species diffusion and energy generation due to chemical reactions in the energy equation. For the gas phase,

$$S(\bar{Q}) = \left\{ \begin{array}{c} 0 \\ \frac{4}{3} \mu u_{,xx} + \frac{\mu}{3} v_{,xy} + \mu u_{,yy} \\ \mu v_{,xx} + \frac{\mu}{3} u_{,xy} + \frac{4}{3} \mu v_{,yy} \\ (u s_{xx} + v s_{xy})_{,x} + (u s_{xy} + v s_{yy})_{,y} - \\ \kappa (T_{,xx} + T_{,yy}) - \left( \rho \sum_{i=1}^N h_i Y_i U_i \right)_{,x} - \\ \left( \rho \sum_{i=1}^N h_i Y_i V_i \right)_{,y} - \sum_{i=1}^N \dot{\omega}_i h_i \end{array} \right\} \quad (8)$$

Where  $N$  is the number of species, the subscript  $i$  is for  $i^{th}$  species,  $h_i$  is the species enthalpy,  $Y_i$  is the mass fraction, and  $\dot{\omega}_i$  is the mass production/destruction rate.

In the above source terms for the gas phase we assume that the Lewis number is identically one,

i.e.  $\rho D_i = \frac{\kappa_i}{C_{p,i}}$ , where  $D_i$  is the binary diffusion

coefficient,  $C_{p,i}$  is the specific heat, and  $\kappa_i$  is the thermal conductivity. Diffusion velocities are

obtained by assuming Fick's law for mass diffusion. Here we neglect the Soret and pressure gradient effects,

$$U_i = -\frac{D}{Y_i} Y_{i,x} \quad \text{and} \quad V_i = -\frac{D}{Y_i} Y_{i,y} \quad (9)$$

In the solid phase, source terms involving these diffusion velocities are neglected. The source term for solid phase is therefore given as:

$$S(\bar{Q}) = \left\{ \begin{array}{c} 0 \\ s_{xx,x} + s_{xy,y} \\ s_{xy,x} + s_{yy,y} \\ (u s_{xx} + v s_{xy})_{,x} + (u s_{xy} + v s_{yy})_{,y} - \\ \kappa (T_{,xx} + T_{,yy}) - \sum_{i=1}^N \dot{\omega}_i h_i \\ \sqrt{\frac{2}{3} \text{tr}(D_{ij}^p D_{ij}^p)} \\ 3s_{xx} \Sigma + 2\Omega_{xy} s_{xy} + 2G \left[ u_{,x} - \Sigma \right] \\ 3s_{xy} \Sigma + 2\Omega_{yx} s_{xy} + 2G \left[ v_{,y} - \Sigma \right] \\ 3s_{xy} \Sigma + \Phi + 2G \left[ \frac{1}{2} (u_{,y} + v_{,x}) \right] \end{array} \right\} \quad (10)$$

Where  $\Phi = \Omega_{xx} s_{xy} + \Omega_{xy} s_{yy} - \Omega_{xy} s_{xx} - \Omega_{yy} s_{xy}$ ,

$\Sigma = \frac{1}{3} u_{i,i}$ ,  $D_{ij}^p$  is the plastic strain rate tensor, and

$\Omega_{ij} = \frac{1}{2} (u_{i,j} + u_{j,i})$  is the spin tensor.

In addition to the above system of equations, the species conservation equations are solved in each phase, given as:

$$(\rho Y_i)_{,t} + (\rho Y_i u)_{,x} + (\rho Y_i v)_{,y} = (\rho D Y_{i,x})_{,x} + (\rho D Y_{i,y})_{,y} + \dot{\omega}_i \quad (11)$$

Mass production rates are determined by phenomenological chemical kinetic expressions.

Assuming that the reactions are thermodynamically simple:

$$\dot{\omega}_i = W_i \sum_{l=1}^M \left[ (\nu_{i,l}'' - \nu_{i,l}') k_f^l \prod_{j=1}^N \left( \frac{\rho Y_j}{W_j} \right)^{\nu_{j,l}'} \right] \quad (12)$$

Where  $M$  is the number of reactions,  $W_i$  is the molecular weight of  $i^{\text{th}}$  species, and  $\nu_{i,l}'$  and  $\nu_{i,l}''$  are the stoichiometric coefficients of the reactant and product, respectively.

The reaction rate is based on an Arrhenius form, having unit of  $\text{s}^{-1}$ :

$$k_f = A \exp \left[ \frac{-E_a}{R_u T} \right] \quad (13)$$

Where  $A$  is the pre-exponential factor,  $E_a$  is the activation energy, and  $R_u$  is the universal gas constant. The expression for  $i^{\text{th}}$  species enthalpy is:

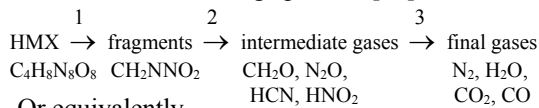
$$h_i = \Delta h_{f,i}^o + \int_{T_o}^T C_{p,i} dT \quad (14)$$

Where  $\Delta h_{f,i}^o$  is the enthalpy of formation for  $i^{\text{th}}$  species at reference temperature,  $T_o$ , taken as 298 K.

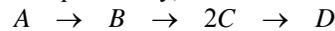
### Chemical Kinetic Model

A reduced kinetic model proposed by McGuire and Tarver [11] is implemented to model the reactions in the condensed and gas phases. We are interested only in how qualitatively distinct species of a reduced kinetics model manifest themselves during hot-spot formation and the subsequent ignition of the reactive material in a viscoplastic void collapse process.

The thermal decomposition of HMX can be modeled as a three stage process [11]:



Or equivalently,



The three major groups of irreversible rate-controlling steps in the HMX decomposition process are (1) unimolecular endothermic breaking of C-N and / or N-N bonds to produce methylene nitramine and other higher molecular weight fragments; (2) weakly exothermic unimolecular decomposition of these condensed phase fragments to produce intermediate gases:  $\text{CH}_2\text{O} + \text{N}_2\text{O}$  or

$\text{HCN} + \text{HNO}_2$ ; and (3) highly exothermic bimolecular gas phase reactions between these intermediate gases to produce stable reaction products  $\text{N}_2$ ,  $\text{H}_2\text{O}$ ,  $\text{CO}_2$ ,  $\text{CO}$ , etc. Note that of these three mechanisms the first occurs in the condensed phase, the last two reactions occur in gas phase. For vapor reactant (species B) to exist in the gas pore, formation of species B in the solid phase is allowed to advect into the gas phase through the boundary condition apply at the gas phase's ghost cells.

### Constitutive Relations

The equations governing the material deformation appropriate for high strain rate applications can be formulated by assuming that the volumetric or dilatational response is governed by an equation of state while the shear or deviatoric response obeys a conventional flow theory of plasticity. The equation of state for solid phase is of Mie-Grüneisen form:

$$p(e, V) = \Gamma \frac{e}{V} + f(V) \quad (15)$$

The Grüneisen parameter is defined as:

$$\Gamma = V \left( \frac{\partial p}{\partial e} \right)_V = \frac{\Gamma_0 \rho_0}{\rho}, \quad V = 1/\rho, \text{ and}$$

$$f(V) = \begin{cases} \frac{\rho_0 c_0^2 \phi}{(1-s\phi)^2} \left[ 1 - \frac{\Gamma}{2V} (V_0 - V) \right] & \text{if } V \leq V_0 \\ c_0^2 \left( \frac{1}{V} - \frac{1}{V_0} \right) & \text{if } V > V_0 \end{cases} \quad (16)$$

The yield strength is assumed to be temperature dependent,

$$\sigma_y(T) = \sigma_{yo} \left( \frac{T_m - T}{T_m - T_o} \right) \quad (17)$$

Where the melting temperature [13] is:

$$T_m(\rho) = T_{mo} \left( 1 + \frac{2(\Gamma_o - 1/3)}{\rho} (\rho - \rho_o) \right) \quad (18)$$

and solid phase viscosity is:

$$\mu = \begin{cases} 31.0 \text{ Pa} \cdot \text{s} & \text{if } T < T_m \\ 3.1 \times 10^{-7} \exp(7800/T) \text{ Pa} \cdot \text{s} & \text{if } T \geq T_m \end{cases} \quad (19)$$

Parameters for HMX material properties taken from [14] are given to be:  $\rho_o = 1900 \text{ kg/m}^3$ ,  $C = 1031 \text{ J/kg-K}$ ,  $T_{mo} = 520 \text{ K}$ ,  $s = 2.38$ ,  $\sigma_{yo} = 0.37$

GPa,  $G = 10.0$  GPa,  $\Gamma_0 = 1.1$ , and  $c_0 = 2650$  m/s. For chemical and thermal properties, refer to Tarver et al. [12].

For gas phase, although the JWL equation of state is not accurate at low pressure, we opt to use this form as we expect high gas pressure at the later stage of the pore collapse process, more critical for the problem of interest here. The JWL equation is given as:

$$p(e, V) = A \left( 1 - \frac{\omega}{R_1 V} \right) \exp(-R_1 V) + B \left( 1 - \frac{\omega}{R_2 V} \right) \exp(-R_2 V) + \frac{\omega e}{V} \quad (20)$$

Here  $V = \rho_o / \rho$  and  $A = 38.0651$  Mbar,  $B = 1.2948$  Mbar,  $R_1 = 7.70$ ,  $R_2 = 2.40$ ,  $\omega = 0.33$ . The specific heat for gas phase is based on mass fraction averaged:  $C_p = \sum_{i=1}^N Y_i C_{pi}$ , and similarly for thermal conductivity:  $\kappa = \sum_{i=1}^N Y_i \kappa_i$

### Initial Conditions

The initial conditions describe an equilibrium state between the gas phase and condensed phase. The pore is initially considered to be completely filled with final product gas, species D. Temperatures are given as:

$$T_c = T_g = T_o$$

in the condensed phase, species mass fraction are given to be:

$$Y_A = 1.0; \quad Y_B = Y_C = Y_D = 0.0$$

And in the gas phase:

$$Y_D = 1.0; \quad Y_A = Y_B = Y_C = 0.0$$

Pressures and densities are taken to be:

$$p_g = p_o, \quad \rho_g = \rho_{g,o}$$

where the subscript ‘‘o’’ denotes the reference state with values:

$$T_o = 298 \text{ K}, \quad p_o = 1.0 \text{ Bar}, \quad \text{and} \quad \rho_{o,g} = 0.897 \text{ kg/m}^3$$

### Interfacial Boundary Conditions

The gas-solid interface boundary conditions can be derived from conservation laws by considering a control volume surrounding a segment of the interface. The jump condition in mass conservation is given as:

$$\dot{m}'' = \rho_s (v_{s,n} - v_{i,n}) = \rho_g (v_{g,n} - v_{i,n}) \quad (21)$$

where the interface normal velocity is  $v_{i,n}$  and  $\dot{m}''$  is the interfacial mass flux.

The balance of momentum must be ensured across a solid-gas interface which has zero thickness. This requires that the sum of traction for the two materials vanish:

$$\tilde{t}_{gas} + \tilde{t}_{solid} = \tilde{0} \quad (22)$$

For the gas phase, this traction tensor reduces to just the hydrostatic pressure and viscous stresses. Kinematics boundary conditions are also applied for velocities across the interface.

Temperature continuity at the interface requires:

$$T_i = T_{s,i} = T_{g,i} \quad (23)$$

with interface temperature,  $T_i$  obtained from the balance of heat fluxes due to conduction of the two phases. Only reactant species B is allowed to be advected into the pore in form of reactant vapor. The change in internal energy for gas phase due to incoming species B is:  $Y_B h_{f,B}^o$

### Numerical Method

Spatial discretization with a second order convex ENO scheme [15] and a third order Runge-Kutta for time stepping were implemented. Near the material interface, fluxes are modified to account for the interface boundary conditions [16]. The presence of stiff chemical source terms requires the usage of an operator splitting technique [17]. The resulting ODEs are nonlinear and discretized with a fully implicit first order Euler scheme. For accuracy and stability of the method, the time step for the governing equations is adaptive, with a lower limit for CFL value according to the degree of stiffness in the source term. Subcycling for the ODEs is also employed for enhanced computational speed.

In the solid phase, viscoplastic regularization algorithm [18] is applied to ensure the correct admissible stress states.

The interface is captured using level-set methodology. The transport for the level-set equation is solved using 3<sup>rd</sup>-order ENO scheme along with 3<sup>rd</sup>-order Runge-Kutta time stepping.

### RESULTS

The setup for the problem of interest here is a cylindrical void 5  $\mu\text{m}$  in diameter, centered at

$(0,12.5) \mu\text{m}$  in a  $(12.5 \mu\text{m} \times 25 \mu\text{m})$  domain. Symmetry boundary conditions are applied on left and right, with inflow and outflow boundary conditions on the bottom and top boundaries. Initially a piston is driven into the HMX crystal from the bottom by applying a material velocity of  $1 \text{ km/s}$ , for a pulse of  $1 \text{ ns}$ , see insert sketch of Fig. 1.

Pressure profiles of three probes positioned near the right boundary are shown in Fig. 1. The pore would experience an average shock pressure of about  $6 \text{ GPa}$  with a rise in temperature to around  $700 \text{ K}$  due to shock heating. The lower surface material velocity is calculated to be around  $1.7 \text{ km/s}$ . For a hydrodynamic pore collapse process, the characteristic time,  $\tau_h = d / 2U_m$  is about  $1.5 \text{ ns}$ . In our calculation, the collapse time is around  $2.2 \text{ ns}$ .

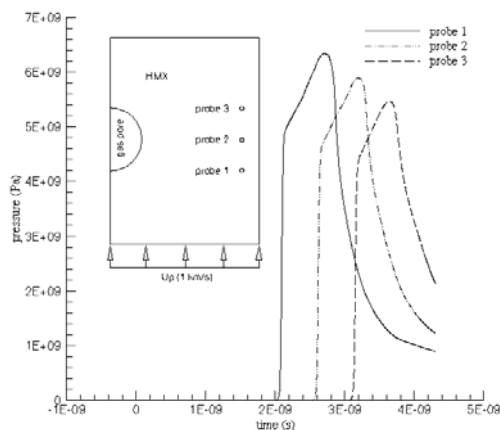


**FIGURE 1. Solid phase pressure profiles.**

As the shock front propagates through the pore, there is a rapid decrease in peak shock pressure from about  $6.3 \text{ GPa}$  to  $5.4 \text{ GPa}$ , within a travel distance of only  $5 \mu\text{m}$ . There is also a clear change in slope toward the top part of pressure profiles. The first effect is due to rarefaction waves from behind attenuating the shock pressure. The second effect, the change in pressure slope, is due to viscoplastic regularization formulation, where stresses are allowed to relax to the yield surface and the rate depends on material viscosity. Note that this is not a two wave structure (an elastic precursor followed by the plastic wave.) as the shock wave is strong enough to overrun the elastic wave.

Grid convergence in the solid phase is demonstrated (Fig. 2) utilizing four different mesh densities ( $50 \times 100$ ,  $100 \times 200$ ,  $150 \times 300$ , and

$200 \times 400$ ). Pressure profiles at three locations (Fig. 1) in the domain show only a slight difference for the two fine meshes. We, therefore, assume the finest resolution at  $200 \times 400$  as our grid independent solution.

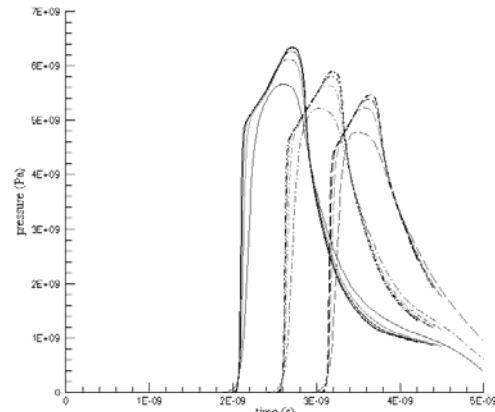


**FIGURE 2. Grid independent study – Solid phase pressure profiles.**

When we plot the profiles for maximum gas phase temperatures (Fig. 3), the solution does not yet seem to converged. For early part of the profiles, up to about  $2.5 \text{ ns}$ , the solutions demonstrate convergence, however at later time, temperature of the finer mesh begins to rise earlier than that of the coarse meshes. From  $2.5 \text{ ns}$  to about  $3.5 \text{ ns}$ , although the differences are noticeable, they are not too drastic. To this point, much of the temperature rise is due to gas compression within the pore as well as mass transfer into the pore in form of vapor species B. Note that there exists gas shocks present within the pore.

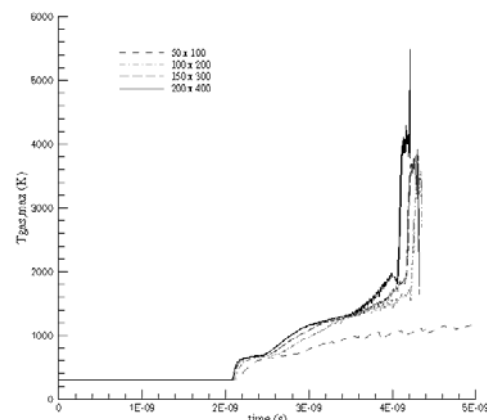


**FIGURE 3. Grid independent study - Maximum gas phase temperature.**

Above  $3.5 \text{ ns}$ , the solutions from the four meshes show drastic differences in term of the steepness of temperature rise and peak magnitude. This is due to the fact that we have a chemically reactive system that begins to react given sufficient rise in temperature.

For a truly converged solution, one would need to have a time step that at least has the same order of magnitude of the time step of the fastest reaction within the system. This would require orders of magnitude higher resolution and is clearly too computationally expensive at present.

A similar conclusion is reached when we plot average gas pressure versus time (Fig. 4). For the coarsest resolution ( $50 \times 100$ ), the rise in pressure is only an order of magnitude above the initial condition, whereas for the finest mesh, pressure rise can reach up to 1000 bars. The drop-off toward the end is due to the fact that there is not enough resolution in the collapsing pore.

Even with this large rise in gas pressure, it is still lower than the yield strength of the solid phase to cause a reversal of plastic flow. However, as will be shown later, this provides enough resistance to slow down the pore collapse process for the critical gas phase energy release to transfer to the solid phase. For subsequent discussions, we will use the results from the  $200 \times 400$  mesh size calculations.

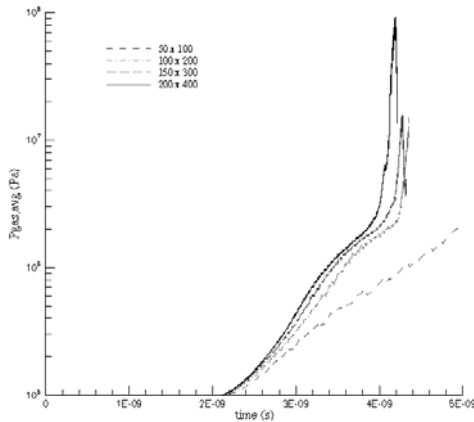


**FIGURE 4. Grid independent study – Average gas phase pressure.**

Figure 5 shows profiles of maximum gas and solid phase temperature, along with average mass fraction of gaseous species within the pore. The initial rise in solid phase temperature up to about  $1.2 \text{ ns}$  is due to shock heating. Thereafter, until about  $2.5 \text{ ns}$ , the drop off is due to the finite shock

pulse width giving rise to shock attenuation. Gas pore temperature starts to increase when the shock hits the lower surface of the pore, around  $2.1 \text{ ns}$ , up to about  $3.6 \text{ ns}$ . The increase is also due to interfacial mass flux coming from the solid phase.

Note that from about  $2.8 \text{ ns}$  to around  $4 \text{ ns}$ , the maximum gas phase temperature is higher than that of solid phase. The higher rise in temperature is due mostly to gas phase compression along with interface mass flux coming from the solid phase. There is negligible exothermic reaction at this temperature.

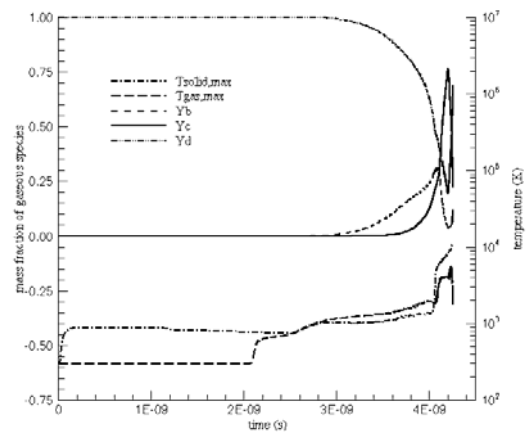


**FIGURE 5. Maximum temperature in solid and gas phases in lower profiles. Average gaseous species mass fraction in the upper profiles.**

Just beyond  $4 \text{ ns}$ , there is a rapid rise in both gas and solid phase temperature with gas phase temperature reaching  $4000 \text{ K}$  around  $4.2 \text{ ns}$ . The solid phase temperature rises above that of the gas phase, due to the formation of a solid phase shock stem near the surface, a region where solid phase has fully undergone conversion from species A to B, i.e., does not require any more energy for endothermic reaction. The third reaction starts to kick in around  $4.2 \text{ ns}$  as seen in the abrupt rise of species D mass fraction, along with the abrupt rise of gas temperature (maximum around  $5500 \text{ K}$ ). One can also see the rapid consumption of species B and C as well. From this point on, the rate of vapor reactant supplied to the gas pore cannot keep up with the consumption rate. Therefore, for gas phase chemical energy release, the rate limited process is the vapor reactant mass flux at the gas-solid interface, as expected.

Pore collapse under the current dynamic shock loading condition is not a symmetric process about the center (Fig. 6). This holds especially true if one

considers the fact that gas present within the pore does not immediately reach an equilibrium state for the duration of pore collapse process. As the planar shock impacts the lower pore surface, the interface begins to accelerate, but at the same time, the gas is being compressed around this region as well. Although gas pressure is still a few orders of magnitude smaller than that of solid pressure, it provides a resistance to somewhat slow down the collapse process in this region.

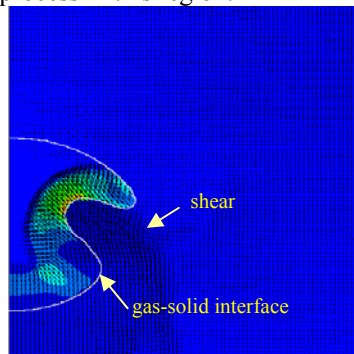


**FIGURE 6. Close-up view of gas phase pressure and velocity field show shock formation within the pore.**

Once the shock in the solid phase moves up to the side of the pore, the transverse impingement on the side surface causes a rapid collapse process, giving substantial rise in temperature due to viscoplastic heating compared to bulk shock heating. This is critical as the temperature in this region can be high enough for solid phase transformation, the first endothermic reaction to take place which will supply the pore with reactant vapor. Another interesting feature resulting from irregular pore collapse is shear banding mechanism as also shown in the figure. This does give rise to localized thermal field slightly away from the pore surface.

Contour plots of species B (left) and C (right) mass fractions (Fig. 7) show the depletion of species B and the production of species C. One can see clearly the complete destruction of species B near the solid-gas interface and the maximum production of species C in the same region. This is in essence a flame front due to the exothermic reaction. Elsewhere in the pore, the temperature is not high enough for spontaneous 2<sup>nd</sup> reaction to take place, although there is a continuous

production of species C. Production of species D, the last exothermic reaction, with locally much smaller reaction rate, is minimal at this point in time. In the region around the interface where gas phase reactions occur, the energy is being continuously transferred to the solid phase. This results in a complete conversion of species A to species B as shown in the left of figure 7.

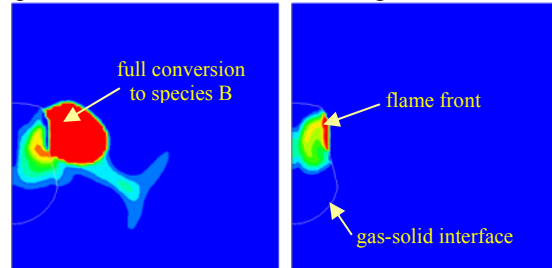


**FIGURE 7. Close-up view shows destruction of species B (left) inside the pore as well as production of species C (right) – Notice thin layer adjacent to pore surface.**

In figure 8, we show a time sequence of pressure contours. From the shape of the gas pore, the collapse process is initially not symmetric about the pore center, and in later time, when the gas pore pressure equilibrated, it becomes symmetrical. As the shock plane impacts the lower pore surface, it produces an essentially free surface since the initial gas pressure is negligible compare to shock pressure. The rarefaction wave created by this free surface travels back into the compressed material, attenuating the shock profile close to the pore surface. In the middle plot on second row, a Mach stem (next to pore surface) starts to form as the gas pore begins to react. This is close to the location where shear banding occurs. However, for calculation without chemistry, shear banding alone is not a significant effect. So there is a coupling of the release of chemical energy inside the pore to the solid phase energy at the interface. In subsequent plots, the Mach stem grows stronger, becomes circular, and begins to detach from the pore surface. From this point on, the Mach stem grows stronger than the leading shock and it will eventually catch up and over-take the leading shock. Again, the speed of the shock is enhanced due to the medium already being compressed.

Figure 9 shows a close-up view of the shock

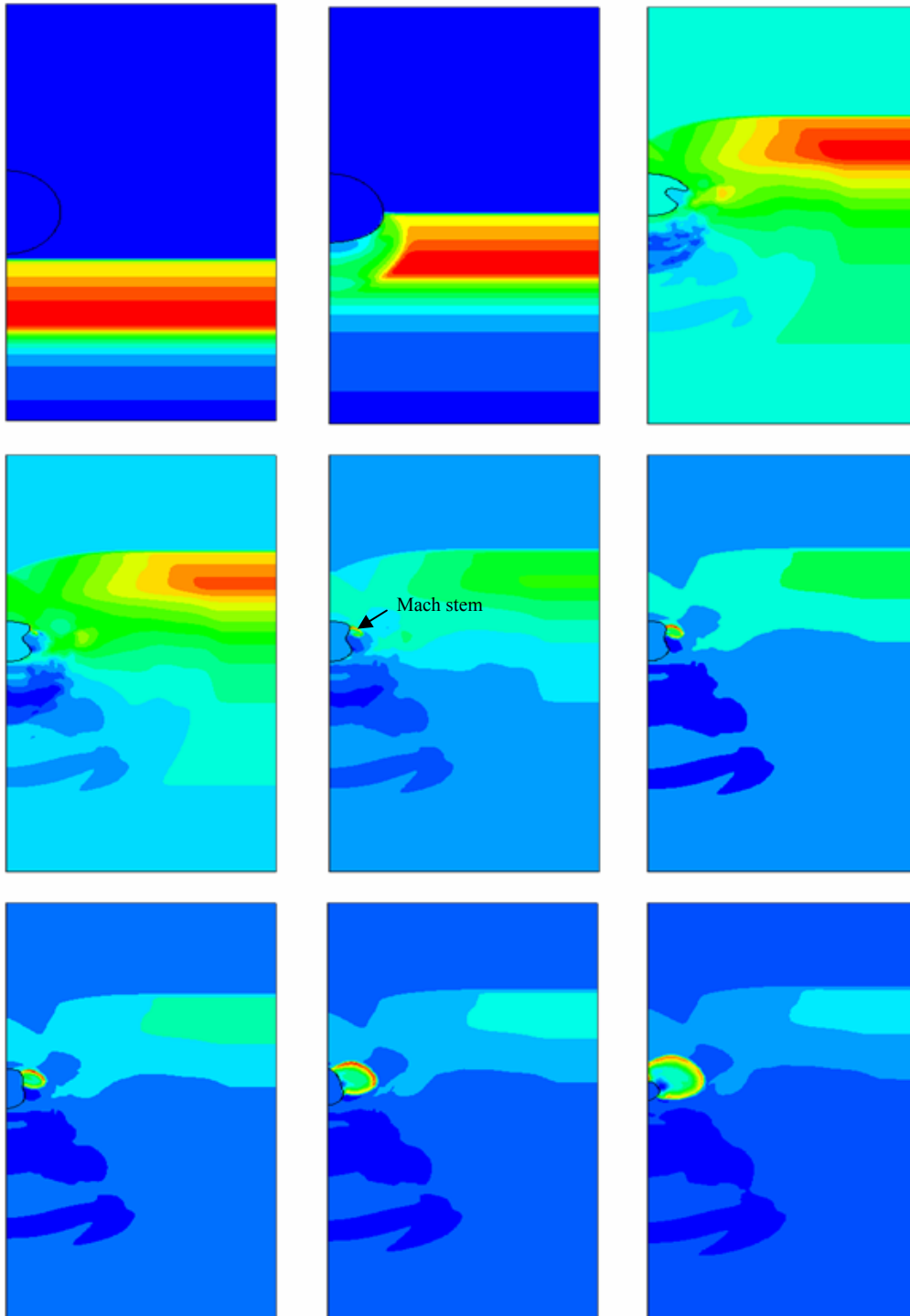


**FIGURE 8. Sequence of pressure contours show Mach stem formation due to gas phase chemical energy release around the collapsing pore.**

detaching from the pore surface, as well as the velocity vector field. The pressure field behind the

Mach stem is of order  $10 \text{ GPa}$ , causing the pore to continue to collapse since the gas pressure,

(although 3 orders of magnitude higher than initial value) is not enough to cause a reversal in plastic flow. The pore shape at this stage is rather symmetric. Note that within this circular shock, full conversion from solid species A to B is completed (Fig. 7). This in turn continuously supplies the pore with fresh vapor reactant in form of species B.

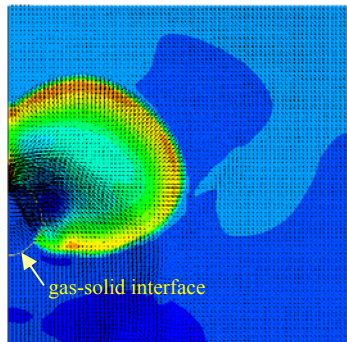


**FIGURE 9. Close-up view of shock formation as it detaches from the pore surface.**

## CONCLUSION AND REMARK

### Conclusion

A mesoscale simulation is carried out to examine shock-initiation due to gas phase reaction at site of cylindrical pore within an HMX crystal. Systems of conservation laws for both solid and gas phases are solved along with species conservation from a reduced set of chemical kinetic model. Mass, momentum, and energy transfer between phases are applied explicitly at the solid-gas interface using physical boundary conditions. It is found that these processes provide the necessary and critical bridge for chemical energy generated within the gas pore to transfer to the solid phase.

Although we observe a flame front near a region of the solid-gas interface, the interface regression rate is limited to a mass diffusion velocity. Therefore, the outward propagation of the interface due to surface burning is small compare to the pore collapse rate. The transfer of thermal energy to the solid layer adjacent to the pore gives rise to temperature which is sufficient for the continuing first endothermic reaction in the solid phase to take place. This in turn, provides fresh vapor reactant to the gas pore, necessary for continuing combustion. The feed back cycle is limited to the mass flow rate of vapor reactant

coming into the pore. The gas phase chemical energy release transferred to the solid phase, causes a rise in the solid phase pressure. Mach stem formation is observed around the shear banding region. Although shear banding is not the cause of shock formation, it contributes to the localized elevated thermal energy. When the shock gathers enough strength, it detaches from the pore surface and propagates outward.

With respect to the reversal of plastic flow around the pore observed in other idealized spherical viscoplastic models, this study shows that the gas pore pressure never reaches values above the pressure field in the solid phase around the pore. Although the gas phase pressure could reach up to 3 orders of magnitude higher than initial value, it never exceeds the surrounding solid pressure. In theory, the gas pressure could be very high as the pore collapses, however, the resolution of the pore is poor towards the end of its life and therefore numerical dissipation could be significant. On the other hand, the physical reasoning is that with continuous transfer of gas phase chemical energy to solid phase, the solid phase pressure around the interface also rises, which, it appears the gas pressure could not overcome.

It is shown in this study that viscoplastic pore collapse is a non-equilibrium process. Although the characteristic collapse time is close to the hydrodynamic mode as categorized by other works, the process itself is not hydrodynamic. Previous works rely on an idealized spherical pore to categorize pore collapse regimes with gas phase pressure and temperature taken from bulk values, similarly for the solid phase. The collapsing process is quite complex however and non-equilibrium, competing processes must be accounted for.

### Remark and Future Work

Interface energy transfer is formulated based only on the balance of conduction heat fluxes between the gas and solid phases. It is shown that the gas phase temperature is well above 1000 K in the later stage of pore collapse process when the gas shock propagates away from the pore surface. Radiative heat transfer could play a role in increasing the solid phase temperature.

Interfacial mass flux which accounts for the vapor reactant coming into the pore is based on

convective flux applied at the interface. The available vapor reactant is taken from solid phase and applied to the ghost cells of gas phase. More rigorous interfacial mass flux treatment is needed.

The validity of the JWL equation of state for the initial gas phase is questionable. The initial gas phase pressure buildup although not critical, is important in determining how the pore shape evolves. This plays a key role in where viscoplastic heating is dominant. For the solid phase, the validity of the Mie-Grüneisen equation of state for a re-shocked material is unknown. This issue is relevant to the formation of the Mach stem in the shocked solid phase.

In term of numerics, subcycling of the ODEs along with adaptive time stepping for governing equations, many time iterations,  $O(10000)$  are required. This could give rise to significant round-off error.

## REFERENCES

1. Bowden, F. P. and Yoffe, A. D., "Initiation and growth of explosions in liquids and solids," Cambridge University Press, Cambridge (1952).
2. Frey, R., "The initiation of explosives by rapid shear," *Seventh Symposium (International) on Detonation*, Naval Surface Weapons Center, NSWC MD, pp. 36-42 (1981).
3. Kipp, M.E., "Modeling granular explosive detonations with shear band concepts," *Eighth Symposium (International) on Detonation*, Naval Surface Weapons Center, Albuquerque, pp. 35-41 (1985).
4. Mader, C., "Initiation of detonation by the interaction of shock with density discontinuity," *The Physics of Fluids*, Vol. 8, No. 10, pp. 1811-1816 (1965).
5. Carroll, M. M. and Holt, A. C., "Static and dynamic pore-collapse relations for ductile porous materials," *J. Appl. Phys.*, Vol. 43, No. 4, pp. 1626-1636 (1972).
6. Khasainov, B. A., Borisov, A. A., Ermolaev, B. S., and Korotkov, A. I., "Two phase viscoplastic model of shock initiation of detonation in high density pressed explosives," *Seventh Symposium (International) on Detonation*, Naval Surface Weapons Center, NSWC MD, pp. 435-447 (1981).
7. Butler, P. B., Kang, J., and Baer, M.R. "Hot spot formation in a collapsing void of condensed-phase, energetic material," *Ninth Symposium (International) on Detonation*, Portland, Oregon, pp. 906-917 (1989).
8. Partom, Y., "Void collapse model for shock initiation," *Seventh Symposium (International) on Detonation*, Naval Surface Weapons Center, NSWC MD, pp. 506-516 (1981).
9. Frey, R., "Cavity collapse in energetic materials," *Eighth Symposium (International) on Detonation*, Naval Surface Weapons Center, Albuquerque, pp. 68-80 (1985).
10. Starkenberg, J., "Ignition of solid high explosive by the rapid compression of an adjacent gas layer," *Seventh Symposium (International) on Detonation*, Naval Surface Weapons Center, NSWC MD, pp. 3-16 (1981).
11. McGuire, R.R. and Tarver, C.M., "Chemical decomposition models for the thermal explosion of confined HMX, TATB, RDX, and TNT explosives," *Seventh Symposium (International) on Detonation*, Naval Surface Weapons Center, NSWC MD, pp. 56-64 (1981).
12. Tarver, C.M., Chidester, S.K., and Nichols, A.L. III, "Critical conditions for impact- and shock-induced hot spots in solid explosives," *J. Phys. Chem.*, Vol. 100, pp. 5794-5799 (1996).
13. Belytschko, T., Liu, W. K., and Moran, B., *Nonlinear Finite Elements for Continua and Structures*, Wiley (2000).
14. Menikoff, R. and Sewell, T. D., "Constituent properties of HMX needed for meso-scale simulations," LA-UR-00-3804.
15. Liu, X.-D. and Osher, S., "Convex ENO high order schemes without field-by-field decomposition or staggered grids," *J. Comp. Phys.*, Vol. 142, pp. 304-330, (1998).
16. Tran, L. and Udaykumar, H.S. "A particle-level-set based sharp interface Cartesian grid method for impact, penetration, and void collapse," *J. Comp. Physics.*, Vol. 193, Issue 2, pp. 469-510, (2004).
17. Strang, G., "On the construction and comparison of difference schemes," *SIAM J. Numer. Anal.*, Vol. 5, pp. 506-517 (1968).
18. Simo, J.C. and Hughes, T.J.R., *Computational Inelasticity*, Springer (2000).

NO. OF  
COPIES ORGANIZATION

1 DEFENSE TECHNICAL  
(PDF INFORMATION CTR  
ONLY) DTIC OCA  
8725 JOHN J KINGMAN RD  
STE 0944  
FORT BELVOIR VA 22060-6218

1 US ARMY RSRCH DEV &  
ENGRG CMD  
SYSTEMS OF SYSTEMS  
INTEGRATION  
AMSRD SS T  
6000 6TH ST STE 100  
FORT BELVOIR VA 22060-5608

1 DIRECTOR  
US ARMY RESEARCH LAB  
IMNE ALC IMS  
2800 POWDER MILL RD  
ADELPHI MD 20783-1197

3 DIRECTOR  
US ARMY RESEARCH LAB  
AMSRD ARL CI OK TL  
2800 POWDER MILL RD  
ADELPHI MD 20783-1197

ABERDEEN PROVING GROUND

1 DIR USARL  
AMSRD ARL CI OK TP (BLDG 4600)

NO. OF  
COPIES ORGANIZATION

ABERDEEN PROVING GROUND

14 DIR USARL  
AMSRD ARL WM BD  
J COLBURN  
B HOMAN  
K MCNESBY  
AMSRD ARL WM T  
P BAKER  
AMSRD ARL WM TA  
R FREY  
AMSRD ARL WM TB  
S AUBERT  
A BIRK  
R EHLERS  
B MCANDREW  
T PIEHLER  
R SKAGGS  
L TRAN  
AMSRD ARL WM TD  
S BILYK  
T BJERKE